Nanoscale

Accepted Manuscript

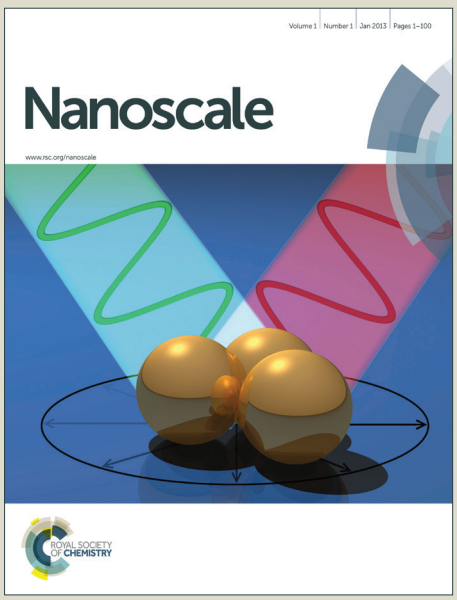

ROYAL SOCIETY OF CHEMISTRY

www.rsc.org/nanoscale

Nanoscale

ARTICLE

Nanostructured p-type CZTS thin films prepared by facile solution process for 3D p-n junction solar cells

Received 00th January 20xx,
Accepted 00th January 20xx

DOI: 10.1039/x0xx00000x

www.rsc.org/

Si-Nae Park,‡[a] Shi-Joon Sung,‡[a] Jun-Hyoung Sim,[a] Kee-Jeong Yang,[a] Dae-Kue Hwang,[a] JunHo Kim,[b] Gee Yeong Kim,[c] William Jo,[c] Dae-Hwan Kim*[a] and Jin-Kyu Kang*[a]

Nanoporous p-type semiconductor thin films are prepared by simple solution-based process with appropriate thermal treatment and three-dimensional (3D) p-n junction solar cells fabricated by depositing n-type semiconductor layers onto the nanoporous p-type thin films shows considerable photovoltaic performance compared with conventional thin film p-n junction solar cells. Spin-coated p-type Cu_2ZnSnS_4 (CZTS) thin films prepared using metal chlorides and thiourea shows unique nanoporous thin film morphology, which is composed of the cluster of CZTS nanograins with 50~500 nm, and the obvious 3D p-n junction structure is fabricated by the deposition of n-type CdS on the nanoporous CZTS thin films by chemical bath deposition. The photovoltaic properties of 3D p-n junction CZTS solar cells is dominantly affected by the scale of CZTS nanograins, which is easily controlled by sulfurization temperature of CZTS precursor films. The scale of CZTS nanograins determines the minority carrier transportation within 3D p-n junction between CZTS and CdS, which are closely related with photocurrent of series resistance of 3D p-n junction solar cells. 3D p-n junction CZTS solar cell with nanograins below 100 nm shows power conversion efficiency of 5.02%, which is comparable with conventional CZTS thin film solar cells.

Introduction

Solution-based inorganic solar cells have attracted a great deal of interest due to the low cost and high-throughput manufacturing associated with solution process.[1] However, in the case of general solution-based inorganic solar cells, the quality of absorber materials is generally inferior to vacuum-based absorbers due to the usage of solvent and many additives, limited grain growth of absorber materials, and so on. Therefore, the photovoltaic performance of solution-processed inorganic solar cells are not good as vacuum-based solar cells. In order to overcome this limitation of solution-processed solar cells, various three-dimensional (3D) structures of solar cell devices were widely investigated by many researchers.[2,3] The advantage of using nanostructured materials is that light absorption and charge migration no longer occur in one material but are taken care of by two or more different materials, which are interconnected on a nanometer scale. In this way the migration distance of the minority carriers is reduced several orders of magnitude, which reduces recombination of electrons and holes.[4-7] 3D solar cells are normally based on the n-type nanostructured materials, which has various platforms of nanostructure, such as nanoparticle,[8] nanorod,[9,10] nanowire,[11-14] and so on. In general, nanostructured n-type semiconductor materials was firstly fabricated and p-type semiconductor materials were deposited on the nanostructured n-type materials for the formation of 3D p-n junction. In this case, the conformal deposition of p-type semiconductors is important and thus solution-based deposition process are generally used for the deposition of p-type semiconductors. However, conventional n-type semiconductors materials are known to be vulnerable to high temperature and thus thermal crystallization process of p-type semiconductors are limited, which leads the deterioration of the material quality of p-type semiconductors. In addition, the conformal deposition of p-type semiconductors on the nanostructured n-type semiconductors is very difficult due to large volume change caused by thermal crystallization process of p-type semiconductors. Therefore, the performance of previously reported 3D solar cells are unsatisfactory considering the complicated fabrication of 3D nanostructured n-type materials. In the case of solution-processed CIGS or CZTS solar cells, various nanostructured n-type materials such as TiO_2 nanoparticle,[15-17] CdS nanowire,[18] and ZnO nanowire[19,20] was also used for the formation of 3D p-n junction with p-type CIGS or CZTS absorbers. However, best performance of 3D solar cells based on CIGS and CZTS is about 6% and 1%, respectively.

[a] Convergence Research Center for Solar Energy, Daegu Gyeongbuk Institute of Science & Technology, Daegu 711-873, Korea. E-mail: monolith@dgist.ac.kr, apollon@dgist.ac.kr
[b] Department of Physics, Incheon National University, Incheon 406-772, Korea.
[c] Department of Physics, Ewha Womans University, Seoul 120-750, Korea.
‡ These authors equally contributed to this work.
Electronic Supplementary Information (ESI) available: [details of any supplementary information available should be included here]. See DOI: 10.1039/x0xx00000x

In our work, we have easily fabricated 3D-structured nanoporous p-type Cu_2ZnSnS_4 (CZTS) thin films by simple spin-coating process with appropriate thermal treatment. CZTS has recently attracted a great amount of interest as a potential material for fabricating a low-cost, low-environmental-impact absorber layer for solar cells. Absorber layers require a direct band gap energy of about ~1.5 eV and an optical absorption coefficient of around 10^5 cm^{-1} so that they can be used for photovoltaic applications. The elements that comprise CZTS are abundant and CZTS is nontoxic, which makes it an ideal candidate to replace $Cu(In,Ga)Se_2$ (CIGS) and CdTe in solar cells, because the elements that comprise CIGS and CdTe are scarce and the materials themselves are toxic.[21-24] In our previous work, we have found that CZTS thin films prepared by spin coating of precursor solution containing thiourea showed unique porous morphology.[25] From further study on the thermal treatment of CZTS thin films, it was found that the scale of nanostructure of CZTS thin films was closely related with sulfurization temperature. By controlling the sulfurization temperature, we have prepared 3D p-n junction CZTS solar cells with different nanostructure scales. We have investigated the photovoltaic properties of the 3D p-n junction solar cells and proposed a new model with p-type nanostructured material-based 3D p-n junction solar cell.

Three samples made from the solution process and a general vacuum process were systematically compared and a very different photo current flowing mechanism of our solution processed sample is proposed. To the best of our knowledge, it is the first working and successful example where a nanostructured p-type chalcogenide absorber, CZTS, was used as a template for the formation of inorganic 3D p-n solar cell. Thanks to the direct formation of 3D p-type absorbers on molybdenum coated substrate, the above-mentioned process temperature limit in typical 3D cells could be overcome. Nanoporous p-type CZTS thin films were firstly deposited on substrates and n-type CdS was uniformly deposited on the nanoporous CZTS thin films. For the preparation of nanoporous CZTS thin films, precursor solution of CZTS was simply spin-coated on the substrate and thermally treated by pre-annealing and sulfurization process. By manipulating the temperature of pre-annealing and sulfurization process, nanoporous CZTS thin films with various nanograin size were automatically fabricated without help of conventional 3D templates. For the formation of 3D p-n junction with CZTS absorbers, CdS buffer layer was deposited on the nanoporous CZTS absorber by simple chemical bath deposition (CBD) method, followed by ZnO sputtering. Because the deposition of CdS by CBD method proceeds under 100 ^oC and does not require any additional high temperature treatment, conformal deposition of CdS buffer layer on nanoporous CZTS is possible. In the case of solution-processed nanoporous CZTS solar cells, the size of CZTS nanograin was a determining factor for photovoltaic properties of 3D p-n junction CZTS solar cells. The transport of minority carriers in p-n junction between nanoporous CZTS and CdS buffer layer would be closely related with the size of CZTS nanograin. Fabricated 3D p-n junction CZTS solar cell with CZTS nanograin below 100 nm showed about 5 % power conversion efficiency (PCE), which is comparable with a conventional sputtered CZTS thin film solar cell.

Experimental

Nanoporous CZTS film preparation

The CZTS precursor thin films were spin-coated onto Mo-coated soda-lime glass substrates. Copper (II) chloride ($CuCl_2$) dehydrate (0.9 M), zinc chloride ($ZnCl_2$) (0.7 M), tin (II) chloride ($SnCl_2$) (0.5 M), and thiourea (4 M) were used as the source chemicals for the precursor solutions. They were completely dissolved in a mixture of deionized water and ethanol to produce the precursor solutions, which were subsequently spin-coated onto molybdenum-coated soda-lime glass substrates at 5000 rpm for 30 s. The spin-coated CZTS precursor thin films were then baked on a hotplate at 350 °C for 5 min to pre-anneal them. The CZTS precursor thin films were spin-coated and pre-annealed twice more to produce suitably thick precursor films, which were then sulfurized at atmospheric pressure in a two-zone tubular furnace. The sulfur evaporated at 300°C, and the sample zone was heated at 540 °C or 570 °C for 30 min. Ar carrier gas at atmospheric pressure was used in the quartz furnace to facilitate the flow of sulfur vapor, and both heating zones were naturally cooled to room temperature. In order to compare the morphological and photovoltaic properties of porous CZTS absorber with thin film CZTS absorber, metal precursor for CZTS were deposited using 99.99% pure Cu (150W DC power), SnS (200W RF power), and ZnS (200W RF power) sputtering targets with a stacking order of Cu/SnS/ZnS/Mo.[26] The sulfurization process for metal precursor for CZTS was same as spin-coated CZTS precursor.

Solar cell fabrication

Chemical bath deposition was used to cover the obtained CZTS thin films with a 40-nm-thick CdS buffer layer, and RF sputtering was used to sequentially deposit a 50-nm-thick intrinsic ZnO layer and a 300-nm-thick Al-doped ZnO layer on top of the buffer layer in order to fabricate solar cells. Thermal evaporation was then used to deposit a 500-nm-thick Al collection grid on top of the device.

Characterization of nanoporous CZTS solar cells

We analyzed the CZTS thin films with various instruments to determine how the pre-annealing temperature affected the chemical composition and morphology of the films and the photovoltaic properties of the CZTS-based solar cells. The surface morphology and chemical composition of the CZTS thin films were observed using scanning electron microscopy (FE-SEM) (Hitachi, SU8200), transmission electron microscopy (FE-TEM) (Hitachi, HF-3300) with focused ion beam (FIB) system (Hitachi, NB5000). The crystalline structure of the CZTS thin films was observed using Raman spectroscopy. The photovoltaic properties of the solar cells were characterized using a source meter (Keithley, 2400) unit and a solar simulator (Newport, 94022A) to simulate 1.5 AM solar

irradiation. EQE measurement was conducted using an incident photon-to-current efficiency (IPCE) measurement system (McScience, K3100). Admittance spectroscopy measurement were performed in the temperature range of 90-300 K with E4980A LCR meter (Agilent Co.), which probes frequencies from 20 Hz to 2 MHz. The measurement was conducted with a temperature error bar of was used for the measurement of ± 0.05K or less. C-AFM is used for measurement of local currents and their mapping on the surface of the CZTS absorber layer. We used a commercial AFM (Nanofocus Inc., n-Tracer, Korea). The Pt/Ir coated-Si cantilevers (Nano sensor, resonance frequency ~85 kHz, tip radius : < 30 nm) were utilized at the contact mode. The local currents and topographic images were obtained simultaneously by applying an external sample dc bias with amplitude of ±0.1 V.[27,28] The Mo bottom electrode of the CZTS sample was connected the voltage source in order to form conductive paths while the top surface connected to the Pt of the tip was grounded. The scanning rate was with 0.5 Hz to obtain clear topological signal. A constant force of 1 nN was applied onto a cantilever for the 5x5 μm^2 scanning area. The wavelength of the AFM laser is 633 nm (E_g = 1.95 eV), which is higher than band gap of CZTS (1.4 eV).

Results and Discussion

In order to compare the morphology between nanoporous and thin film CZTS, SEM was used to examine the surface morphology of spin-coated precursor thin film, solution-processed nanoporous CZTS film and sputtered CZTS thin film (Figure 1). The spin-coated precursor thin film shows porous and rough surface morphology and contains many nanopores, which is not common for conventional precursor films used for preparing inorganic thin films. Unique nanoporous morphology of solution-processed CZTS is closely related with the removal of thiourea and metal chlorides during high temperature pre-annealing process.[25] The sulfurized CZTS precursor films prepared by spin-coating show nanoporous morphology, which comes from the porous morphology of precursor film. In addition, during the sulfurization process of CZTS precursor films, remaining carbon residue and metal chlorides are eliminated by high temperature treatment, which reinforce the porous structure of solution-processed CZTS thin films. However, the size of CZTS nanograin was found to be dependent on the sulfurization temperature of precursor films. In the case of 540 °C sulfurization, nanoporous CZTS film shows many clusters of tiny CZTS nanograins below 100 nm. On the other hand, nanoporous CZTS film sulfurized at 570 °C has cluster structure composed of CZTS nanograins with 300~500 nm. The different size of CZTS nanograins of solution-processed CZTS thin films might be attributed to the different degree of crystallization reaction of precursor films according to the sulfurization temperature. In the case of high temperature sulfurization, sufficient thermal energy is provided to precursor film and thus the sufficient grain growth of CZTS is possible. Unlike solution-processed CZTS thin films, sputtered CZTS thin film shows a typical morphology of thin film absorber. Sputtered CZTS thin film shows dense thin film structure with large CZTS grains above 1 μm. Compared with sputtered CZTS thin film, solution-processed CZTS films shows unique nanoporous and loose morphology due to the thermal degradation of components remaining in precursor films. In order to use CZTS thin films as absorber materials for solar cell, the chemical composition of CZTS thin films is a very important factor.[29] In our work, EDS was used to analyze the chemical composition of solution-processed and sputtered CZTS thin films (Table S1). All of CZTS thin films show Cu-poor and Zn-rich chemical compositions, which is well known requirement for high efficient CZTS solar cells. Spin-coated nanoporous CZTS films showed a relatively lower Cu/(Zn+Sn) and Zn/Sn ratio compared with sputtered CZTS thin films. In order to investigate the distribution of chemical composition inside nanoporous CZTS thin films, auger electron spectroscopy (AES) of S540 was measured (Figure S1). In the full range of thickness of nanoporous CZTS thin films, chemical composition of each elements was constant. We also measured XRD patterns of nanoporous CZTS thin films to confirm the crystalline structure (Figure S2). Both S540 and S570 showed peaks at 28.5, 33.0, 47.4, and 56.3°, corresponding to the single-phase kesterite CZTS structure (JCPDS 26-0575).

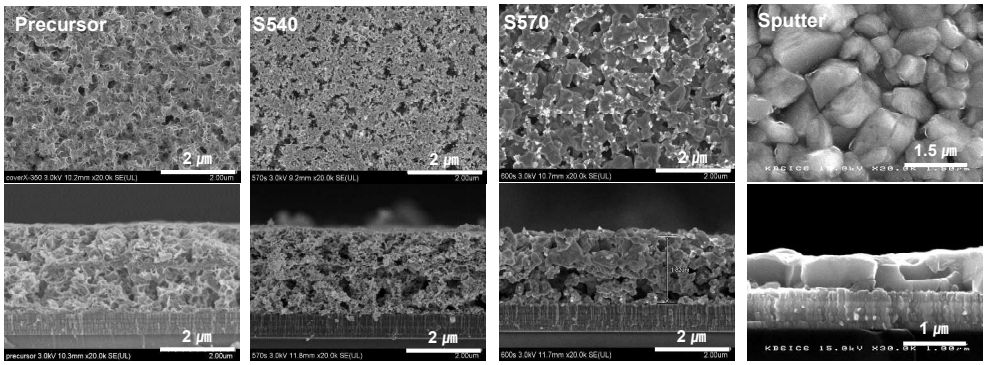

Fig. 1 Top and cross-sectional SEM images of solution-processed precursor film, CZTS films sulfurized at 540 and 570 °C, and CZTS films prepared from sputtering process.

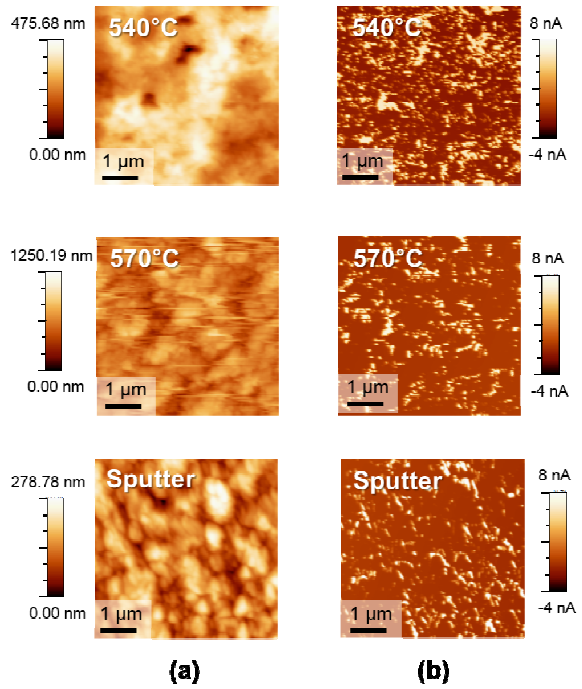

Fig. 2 (a) Topography and (b) local current map images of solution-processed and sputtered CZTS thin films under the positive voltage bias 0.1 V.

In order to compare thin film properties of solution-processed and sputtered CZTS, atomic force microscopy (AFM) instrument were used (Figure 2). For the comparison of grain structure of solution-processed and sputtered CZTS, AFM was used to measure the surface roughness of CZTS thin films (Figure 2(a)). While sputtered CZTS thin film shows root mean square (RMS) roughness of 44.52 nm, solution-processed nanoporous CZTS film sulfurized at 540 and 570 ^{o}C shows RMS roughness of 59.12 and 158.21 nm, respectively.

The higher surface roughness of solution-processed nanoporous CZTS films is closely related with unique cluster structure of CZTS nanograins. For both of nanoporous CZTS with 540 and 570 ^{o}C sulfurization, the surface roughness of nanoporous CZTS films seems to be similar with the size of CZTS nanograins. In order to elucidate the current flow through CZTS thin films, current maps of the nanoporous CZTS films with different nanostructure scales and a sputtered CZTS thin film were investigated by using conductive AFM (C-AFM). Figure 2(b) shows current map images of the nanoporous CZTS films and a sputtered CZTS thin films under positive voltage bias. All of CZTS films shows apparent current flows through grain boundaries in the CZTS films in spite of deposition methods. Kim *et al*. reported that minority carrier electrons form the current route in the GBs in the CZTSSe thin-films.[30] Thus, the conduction channel near GBs can provide a path for the collected minority carriers. In the case of a nanoporous CZTS film with 540 ^{o}C sulfurization, it has many grain boundaries inside the CZTS film due to small CZTS nanograins,

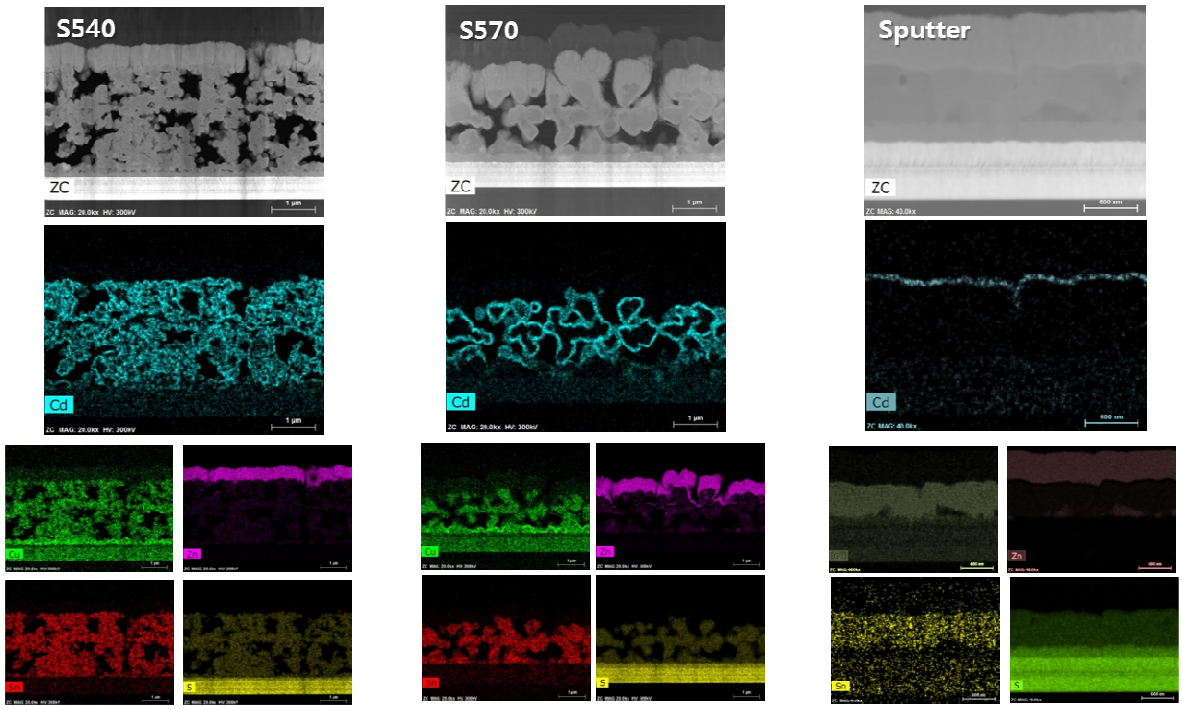

Fig. 3 Cross-sectional TEM & EDS mapping images of nanoporous CZTS solar cells with 540 and 570 ^{o}C sulfurization and thin films CZTS solar cells based on sputtering process. Every elements are assigned by each colors (Cd : sky, Cu: green, Zn : purple, Sn : red, S : yellow).

which can provide a pathway for the transportation of minority carriers. From these results, it was found that solution-processed and sputtered CZTS thin films showed similar current flow behavior under positive bias voltage and thus minority carrier transportation inside CZTS thin films might be closely related with the grain boundaries of the CZTS thin films.

Through pre-annealing and sulfurization process, it was possible to fabricate nanoporous CZTS films with different nanograin structure. In order to fabricate CZTS solar cells, CdS buffer layer was deposited on the prepared nanoporous CZTS films using CBD process, followed by sputtering of ZnO window layer and evaporation of Al top electrode. For the confirmation of p-n junction formation between nanoporous CZTS and CdS, TEM and EDX analysis of CZTS solar cells were conducted (Figure 3). Cross-sectional TEM images of CZTS solar cells using solution-processed nanoporous CZTS films shows cluster structure of CZTS nanograins and there are many voids inside CZTS absorber, which was already confirmed by SEM images of Figure 1. However, solar cell with a sputtered CZTS thin film shows large and dense grain structure without any voids inside CZTS absorber. In order to investigate the distribution of each components in CZTS solar cell, EDX mapping was conducted for the elements of Cu, Zn, Sn, S, Cd, and Mo. From the EDX mapping images, solar cells prepared using solution-processed nanoporous CZTS films show very unique distribution of Cd inside device structure. In the case of conventional thin film CZTS solar cells, CdS buffer layer was only deposited on the top surface of CZTS absorber uniformly. However, in the case of our nanoporous CZTS absorbers, CdS was uniformly distributed on every surface of CZTS nanograins, which is the inverse structure of previously reported 3D solar cell where p type absorbers were formed on the 3D n type materials. Regardless of the size of CZTS nanograin, CdS was evenly deposited on every nanograins of CZTS. Due to the highly porous morphology of solution-processed CZTS films, infiltration and formation of CdS on CZTS surface during CBD process seems to be possible and thus 3D structured CZTS-CdS interface is formed. In the case of 540 ^{o}C sulfurization, the size of CZTS nanograin is very tiny and the interfacial area would be considerably larger than 570 ^{o}C sulfurization, which induces thinner CdS buffer layer on CZTS nanograins. In addition, the size of CZTS nanograin is closely related with the topology of ZnO window layer. In the case of 540 ^{o}C sulfurization, surface roughness of CZTS absorber layer is not so severe, which was confirmed by AFM analysis. Therefore, ZnO window layer is uniformly deposited on the CZTS absorber layer. However, CZTS absorber with 570 ^{o}C sulfurization shows rougher surface than 540 ^{o}C sulfurization and therefore the ZnO window layer is not uniform and shows bumpy structure. The uneven structure of ZnO window layer of CZTS with 570 ^{o}C sulfurization would form a many shunt pass of CZTS solar cells, which might deteriorate the solar cell performance considerably.

Table 1 J-V curves of nanoporous and thin film CZTS solar cells.

	V_{oc} (V)	J_{sc} (mA/cm^2)	FF (%)	PCE (%)	R_s (Ω)	R_{sh} (Ω)
S540	0.52	18.09	53.54	5.02	17.9	2082.0
S570	0.34	1.33	32.22	0.15	284.0	1913.4
Sputter	0.54	15.45	50.79	4.21	44.4	1222.7

In order to investigate the photovoltaic properties of nanoporous and thin films CZTS solar cells, J-V curves of solar cells were measured (Table 1, Figure 4). Solution-processed nanoporous CZTS solar cell with 540 ^{o}C sulfurization shows a cell efficiency of 5.02%, which is superior to that of sputtered CZTS solar cell. In spite of small nanograins and many voids inside nanoporous CZTS absorbers, nanoporous CZTS solar cell shows equivalent performance to conventional sputtered CZTS solar cell. Though open circuit voltage of porous CZTS is inferior to the sputtered CZTS, short circuit current and fill factor is superior to sputtered CZTS. However, solution-processed nanoporous CZTS solar cell with 570 ^{o}C sulfurization shows poor photovoltaic properties compared with that of 540 ^{o}C sulfurization, especially short circuit current is smaller than other samples. The significant difference of short circuit current might be closely related with the minority carrier

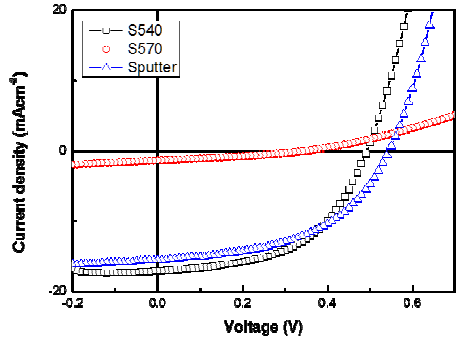

Fig. 4 J-V curves of nanoporous and thin film CZTS solar cells.

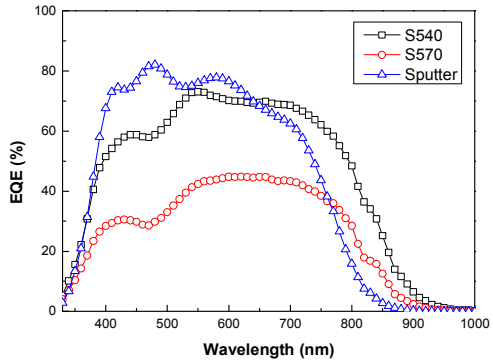

Fig. 5 EQE data of nanoporous and thin film CZTS solar cells.

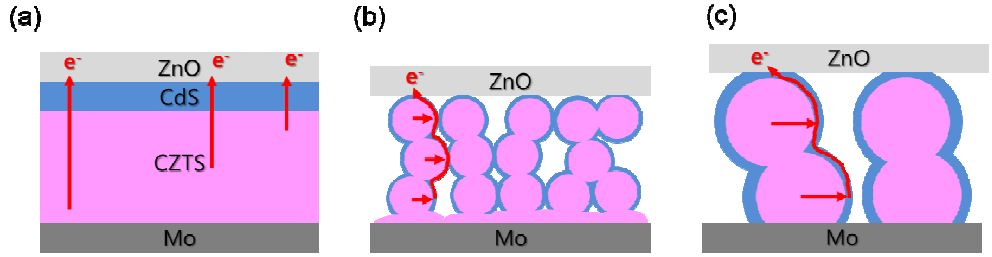

Fig. 6 Schematic diagram of carrier transport in (a) conventional thin films CZTS solar cell, and nanoporous CZTS solar cell with (b) small and (c) large nanograins.

transfer inside p-n junction between CZTS absorber and CdS buffer layer. In the case of 540 °C sulfurization, the scale of 3D p-n junction between CZTS and CdS is about 30~100 nm and the interfacial area between CZTS and CdS is extremely larger than a conventional thin film solar cell. Therefore, the minority carrier generated by photon inside CZTS nanograins just need to move only 100 nm to reach the CdS buffer layer, and thus efficient transfer of photo-generated minority carrier is possible. However, in the case of solution-processed nanoporous CZTS absorber with 570 °C sulfurization, the scale of 3D p-n junction is about 300~500 nm and the minority carrier must travel to CdS buffer layer with much longer distance and thus secure transport of minority carriers between CZTS and CdS is not guaranteed. In addition, nanoporous CZTS thin film with 570 °C sulfurization has larger porosity than 540 °C sulfurization, which might provide additional shunt paths and thus the shorting issue could happens. This difference of minority carrier transport and shorting issue might be closely related with the decreased short circuit current of nanoporous CZTS solar cell with 570 °C sulfurization.

Figure 5 shows EQE measurement data of solution-processed and sputtered CZTS solar cells. For all of solution-processed nanoporous CZTS solar cells, there was evident decrease of EQE below 550 nm compared with sputtered CZTS solar cell, which might be attributed to 3D structured CdS buffer layer located inside the nanoporous CZTS absorber. Unlike conventional thin film CdS buffer layer, interconnected CdS network is uniformly formed on CZTS nanograins and thus some part of absorbed sunlight with the same wavelength of CdS adsorption is absorbed by the CdS network, which induces the decrease of EQE below 550 nm. This unique detriment at short wave length region could be mostly reduced if we use wider band gap buffers like Zn(O,S). Fortunately, solution-processed nanoporous CZTS solar cell with 540 °C sulfurization shows additional light absorption in longer wavelength compared with sputtered CZTS solar cell. Due to the 3D p-n junction between CZTS and CdS, easier transport of minority carriers generated in deep region of CZTS absorber is possible and thus the recombination of minority carriers at longer wavelength is prohibited. Therefore EQE at longer wavelength is higher than that of sputtered CZTS solar cell. In addition, a thick absorber film around 1.8 μm and a naturally formed porous structure could give rise to an enhanced light absorption at longer wavelength as well. Contrary to nanoporous CZTS solar cell with 540 °C sulfurization, solution-processed nanoporous CZTS solar cell with 570 °C sulfurization shows poor EQE regardless of the wavelength. The size of CZTS nanograins with 570 °C sulfurization is not sufficient to transport minority carriers through the interface between CZTS and CdS smoothly and thus most of minority carriers might be involved in charge recombination. This charge recombination is well known for the major cause of EQE deterioration of solar cells.

In the case of solution-processed nanoporous CZTS solar cells, 3D structured p-n junction between CZTS absorber and CdS buffer layer is an important factor for determining the photovoltaic properties of CZTS solar cells. In order to investigate the diode properties of 3D structured p-n junction, dark current density-voltage characteristics were measured with a semiconductor parameter analyzer (Figure S3). Solution-processed CZTS with 540 °C sulfurization shows typical current density-voltage curve of diode. However, solution-processed CZTS with 570 °C sulfurization shows poor diode characteristics. From this result, it was found that the diode characteristics of p-n junction between CZTS nanograins and CdS buffer layer is significantly affected by the size of CZTS nanograin. In the case of solution-processed nanoporous CZTS, the quality of CZTS absorber would be inferior to vacuum-based CZTS absorbers due to the solvent or additives used for the preparation of precursor solution. Therefore the diode characteristics of p-n junction between CZTS nanograin and CdS would be closely related with the scale of p-n junction structure and the size of CZTS nanograin might be a crucial factor for determining the diode characteristics of 3D p-n junction between CZTS and CdS.

In order to investigate 3D p-n junction of nanoporous CZTS solar cells in detail, C-V curves of nanoporous CZTS solar cells and sputtered CZTS solar cells were measured (Figure S4).[31] From the Mott-Schottky plots, the depletion width of p-n junction was calculated. While nanoporous CZTS solar cell with 540 °C sulfurization showed depletion width of 21.8 nm, sputtered CZTS solar cell showed 97.3 nm. The depletion width of nanoporous CZTS solar cell with 540 °C sulfurization correspond with the size of CZTS nanograins. From this result, we can predict that fully-depleted p-n junction between CZTS

and CdS might be possible for nanoporous CZTS solar cell with 540 °C sulfurization. In the case of sputtered CZTS, depletion width of 97.3 nm is shorter than full thickness of CZTS absorber and thus the transportation of minority carriers generated in deep region to CdS layer might be difficult. Therefore photovoltaic properties of sputtered CZTS solar cell are inferior to nanoporous CZTS solar cells with 540 °C sulfurization. In the case of nanoporous CZTS solar cell with 570 °C sulfurization, measurement of proper Mott-Schottky plot was impossible, which might be attributed to the poor p-n junction between larger CZTS grains and CdS layer.

From previous data for nanoporous CZTS solar cells, it was found that the photovoltaic properties of 3D structured p-n junction solar cell is different from conventional thin film solar cells. Figure 6 illustrates the mechanism of carrier transportation inside CZTS solar cells. In the case of conventional CZTS solar cells, photo-generated minority carriers pass through the bulk CZTS absorber to CdS buffer layer (Figure 6(a)). The thickness of CZTS absorber is about 600 nm and thus the sufficient diffusion length of CZTS absorber is required to transport minority carriers smoothly. In this case, high quality CZTS absorber prepared by vacuum-based process is suitable. However, in the case of 3D structured p-n junction solar cell based on nanoporous CZTS (Figure 6(b), (c)), the transport of minority carrier is not determined by bulk CZTS absorber, but determined by the interfacial region between CZTS and CdS. Minority carriers generated from a lot of CZTS nanograins reach interconnected CdS buffer layer and pass through the CdS buffer layer to ZnO window layer. In this case, according to the size of CZTS nanograins, the diffusion length of minority carriers is determined. In the case of smaller CZTS nanograins below 100 nm (Figure 6(b)), photo-generated minority carriers can easily reach CdS buffer layer and the minority carriers move along CdS buffer layer to ZnO TCO layer. However, in the case of larger CZTS nanograins with 300 ~ 500 nm (Figure 6(c)), photo-generated minority carriers must diffuse through CZTS nanograins with longer distance compared with smaller CZTS nanograins and thus there is higher possibility of charge recombination during the diffusion within CZTS nanograins. This dependency of diffusion length on the CZTS nanograin size is very similar with the strategy of previously reported 3D solar cells. In previous study on the nanoscale p-n junction solar cells fabricated by using p- and n-type nanocrystals,[31] it was reported that fully-depleted p-n junction solar cells showed improved photo-current compared with thick p-n junction devices. When excitons reach the vicinity of depletion region from either of the layers, the electrons in the p-type material drift through the junction to the n-type layer; similarly, the holes in the n-type layer also drift to the p-type material due to the electric field at the junction. In the case solution-processed nanoporous CZTS solar cell with 540 °C sulfurization, it could be possible to form fully-depleted p-n junction between CZTS and CdS due to 3D p-n junction structure with several tens of nanometer scale. In addition, in the case of solution-processed CZTS, the quality of CZTS absorber would be inferior to vacuum-based CZTS absorbers due to the solvent or additives used for precursor solution preparation. Therefore the transport of minority carrier inside CZTS nanograins would be limited and thus the distance to CdS buffer layer might be a crucial factor for easier transportation of minority carrier. In the case of low quality absorber material such as solution-processed CZTS, 3D p-n junction between nanoporous CZTS with smaller nanograin and CdS is advantageous for achieving facile transportation of minority carriers in p-n junction and high performance solar cells. Unlike a common-sense view, extremely small grain structured chalcogenides would be more beneficial than μm-sized chalcogenides in processes involving low quality absorbers.

In our work, by using simple solution process, it was possible to fabricate 3D structured nanoporous p-type CZTS thin films. Our preparation method might be a meaningful guideline for the facile fabrication of various nanoporous p-type materials, which would open a new possibility of 3D p-n junction solar cells based on 3D structured p-type materials. If previously reported various n-type materials is applied to our proposed solution-processed nanoporous p-type materials, it will be possible to develop a novel 3D p-n junction solar cell devices with high performance.

Conclusions

In this work, we have prepared unique 3D structured nanoporous p-type CZTS thin films using simple solution process. The nanograin structure of nanoporous CZTS films was easily controlled by the sulfurization temperature of CZTS precursor films. By deposit n-type CdS buffer layer onto the nanoporous CZTS film using simple CBD process, it was possible to fabricate 3D structured p-n junction between CZTS and CdS. Due to the nanoporous structure of solution-processed CZTS thin film, interconnected 3D network CdS buffer layer was uniformly formed on nanoporous CZTS. Photovoltaic properties and diode characteristics p-n junction solar cell based on nanoporous CZTS films shows strong dependency on the size of CZTS nanograin, which might be closely related with the diffusion of minority carriers through the interfacial region. In the case of nanoporous CZTS solar cell with CZTS nanograin below 100 nm, 5.02% PCE was achieved in spite of smaller nanograin and many voids inside CZTS absorber, which resembles the working mechanism of previously reported 3D p-n junction solar cells.

The conclusions section should come in this section at the end of the article, before the acknowledgements.

Acknowledgements

This work was supported by DGIST R&D Program of the Ministry of Education, Science and Technology of Korea (15-BD-05) and the New & Renewable Energy of the Korea Institute of Energy Technology Evaluation and Planning (KETEP) grant funded by the Korea goverment Ministry of Trade, Industry and Energy (no. 20123010010130).

Notes and references

1 A.K. Rath, M. Bernechea, L. Martinez, G. Konstantatos, *Adv. Mater.,* 2011, **23**, 3712.
2 P.V. Kamat, K. Tvrdy, D.R. Baker, J.G. Radich, *Chem. Rev.*, 2010, **110**, 6664.
3 M. Yu, Y.Z. Long, B. Sun, Z. Fan, *Nanoscale*, 2012, **4**, 2783.
4 U. Bach, D. Lupo, P. Comte, J.E. Moser, F. Weissortel, J. Salbeck, H. Spreitzer, M. Gratzel, *Nature*, 1998, **39**, 583.
5 E.W. McFarland, J.A. Tang, *Nature*, 2003, **431**, 616.
6 P. Wang, S.M. Zakeeruddin, J.E. Moser, M.K. Nazeeruddin,T. Sekiguchi, M. Gratzel, *Nat. Mater*., 2003, **2**, 402.
7 A.K. Rath, M. Bernechea, L. Martinez, F.P.G. Arquer, J. Osmond, G. Konstantatos, *Nat. Photonics*, 2012, **6**, 529.
8 C.J. Stolle, T.B. Harvery, B.A. Korgel, *Curr. Opin. Chem. Eng*., 2013, **2**, 160.
9 M. Yu, Y.Z. Long, B. Sin, Z. Fan, *Nanoscale*, 2012, **4**, 2783.
10 T. Song, F. Zhang, X. Lei, Y. Xu, S. Lee, B. Sun, *Nanoscale*, 2012, **4**, 1336.
11 E. Garnett, P. Yang, *Nano Lett*., 2010, **10**, 1082.
12 T.J. Kempa, R.W. Day, S.K. Kim, H.G. Park, C,M. Lieber, *Energy Environ. Sci*., 2013, **6**, 719.
13 K. Sato, M Dutta, N. Fukata, *Nanoscale*, 2014, **6**, 6092.
14 Q. Zhang, S. Yodyingyong, J. Xi, D. Myers, G. Cao, *Nanoscale*, 2012, **4**, 1436.
15 M. Nanu, J. Schoonman, A. Goossens, *Nano Lett*., 2005, **5**, 1716.
16 M. Nanu, J. Schoonman, A. Goossens, *Adv. Mater*., 2004, **16**, 453.
17 K. Tanaka, M. Kurokawa, K. Moriya, H. Uchiki, *J. Alloys Compd*., 2013, **571**, 98.
18 W.C. Kwak, S.H. Han, T.G. Kim, Y.M. Sung, *Cryst. Growth Des*., 2010, **10**, 5297.
19 I.O. Acik, A. Katerski, A. Mere, J. Aarik, A. Aidla, T. Dedova, M. Krunks, *Thin Solid Films*, 2009, **517**, 2443.
20 D. Lee, K. Yong, *J. Phys. Chem*. C, 2014, **118**, 7788.
21 J.J. Scragg, P.J. Dale, L.M. Peter, G. Zoppi, I. Forbes, *Phys. Stat. Sol. B*, 2008, **245**, 1772.
22 S.C. Riha, B.A. Parkinson, A.L. Prieto, *J. Am. Chem. Soc*., 2009, **131**, 12054.
23 T. Tanaka, T. Nagatomo, D. Kawasaki, M. Nishio, Q. Guo, A. Wakahara, A. Yoshida, H. Ogawa, *J. Phys. Chem. Solids*, 2005, **66**, 1987.
24 H. Katagiri, *Thin Solid Films*, 2005, **480-481**, 426.
25 S.N. Park, S.J. Sung, D.H. Son, D.H. Kim, M. Gansukh, H. Cheong, J.K. Kang, *RSC Adv*., 2014, **4**, 9118.
26 K.J. Yang, J.H. Sim, B. Jeon, D.H. Son, D. H. Kim, S.J. Sung, D.H. Hwang, S. Song, D.B. Khadka, J. Kim, J.K. Kang, *Prog. Photovolt: Res. Appl.*, http://dx.doi.org/10.1002/pip.2500.
27 R.H. Shin, A.R. Jeong, W. Jo, *Curr. Appl. Phys*., 2012, **12**, 1313.
28 R.H. Shin, W. Jo, D.W. Kim, J.H. Yoon, S. Ahn, *Appl Phys. A*, 2011, **104**, 1189.
29 K. Tanaka, Y. Fukui, N. Moritake, H. Uchiki, *Sol. Energy Mater. Sol. Cells*, 2011, **95**, 838.
30 G.Y. Kim, J.R. Kim, W. Jo, D.H. Son, D.H. Kim, J.K. Kang, *Nanoscale Res. Lett*., 2014, **9**, 10.
31 U. Dasgupta, S.K. Saha, A.J. Pal, *Sol. Energy Mater. Sol Cells*, 2014, **124**, 79.